Gutzwiller approximation for indistinguishable interacting Brownian particles on a lattice

Adam Deaker and Michael W. Jack[*]

Department of Physics, University of Otago, P.O. Box 56, Dunedin 9054, New Zealand

Nonequilibrium Brownian systems can be described using a creation and annihilation operator formalism for classical indistinguishable particles. This formalism has recently been used to derive a many-body master equation for Brownian particles on a lattice with interactions of arbitrary strength and range. One advantage of this formalism is the possibility of using solution methods for analogous many-body quantum systems. In this paper, we adapt the Gutzwiller approximation for the quantum Bose-Hubbard model to the many-body master equation for interacting Brownian particles in a lattice in the large-particle limit. Using the adapted Gutzwiller approximation, we numerically explore the complex behavior of nonequilibrium steady-state drift and number fluctuations throughout the full range of interaction strengths and densities for on-site and nearest-neighbor interactions.

I. INTRODUCTION

Models of interacting Brownian particles on a lattice have been used to describe a range of nonequilibrium physical systems including molecular motors [1–3], colloidal particles [4], and traffic flow [5–7]. A number of models incorporating different types of particle interactions have been proposed, including the asymmetric simple exclusion process (ASEP) [1] and the zero-range process (ZRP) [8]. Recently, a many-body master equation for interacting Brownian particles on a lattice was derived, which generalizes these models to arbitrary interaction strength and range [9]. The many-body master equation is formulated using an operator formalism for indistinguishable classical particles. One advantage of this operator formalism is the ability to exploit solution methods from quantum many-body physics. In this paper, we adapt the Gutzwiller approximation used for the quantum Bose-Hubbard model to treat the case of classical Brownian particles on a lattice. We then use it to explore the transition from noninteracting to strongly interacting particles in the case of on-site and nearest-neighbor interactions.

One of the simplest models of interacting Brownian particles on a lattice is the ASEP [1]. In the ASEP, there is a strong repulsive interaction between particles, which prevents particles from hopping to an occupied neighboring site. Due to the simplicity of the ASEP, analytical solutions are obtainable, and it has been applied to many systems such as polymerization of nucleic acids [10,11] and molecular motors [1,3]. Another model for interacting particles on a lattice is the ZRP [8,12]. In the ZRP, there is an interaction between particles on the same site, and this gives rise to hopping rates that are a function of the number of particles at the departure site. Important properties of the ZRP are that the nonequilibrium steady state has a factorized form and can be mapped to the ASEP [8]. The ZRP has many applications including modeling polymer dynamics [13] and sandpile dynamics [14]. A generalization of the ASEP and ZRP is the misanthrope process [15], where the hopping rates are a function of the number of particles at the departure and arrival sites. The misanthrope process has applications in traffic modeling [5,16].

Recently, a many-body master equation describing interacting Brownian particles on a lattice was derived [9]. The many-body master equation describes particles interacting via a "top-hat" interaction potential of arbitrary interaction strength and range and thus generalizes many of the existing models. The many-body master equation is formulated using a creation and annihilation operator formalism for classical particles [17,18] which treats the Brownian particles as indistinguishable bosons. This formalism means that we can no longer follow the trajectory of an individual particle, but it helps reveal the collective behavior, which is of interest here. The many-body master equation is not analytically solvable in general, and exact numerical solutions quickly become unviable for large numbers of particles and sites.

In quantum mechanics, the Bose-Hubbard model describes bosonic quantum particles with on-site interactions hopping on a discrete lattice [19]. Thus the Bose-Hubbard model represents an analogous quantum model to the many-body master equation for Brownian particles. Many methods have been developed to explore the Bose-Hubbard model, including Bogoliubov theory [20] and the Gutzwiller approximation [21,22]. In particular, the Gutzwiller approximation has been used to explore the superfluid-to-Mott-insulator transition of the Bose-Hubbard model [22] and to demonstrate the formation of Mott-insulator shells in nonuniform systems [23]. Because of the formal similarity of the Bose-Hubbard model to the recently derived many-body master equation for Brownian particles [9], adapting these methods to Brownian systems seems promising.

In this paper we show how to adapt the Gutzwiller approximation from quantum mechanics to the Brownian case.

---
*michael.jack@otago.ac.nz

Using the adapted Gutzwiller approximation, we then treat the transition from noninteracting to strongly interacting particles of the many-body master equation for Brownian systems on a lattice in the case of on-site and nearest-neighbor interactions. This has not been explored previously in the literature.

This paper is structured as follows. In Sec. II we briefly review the operator formalism for classical particles and the many-body master equation for interacting Brownian particles on a lattice. In Sec. III we show how to adapt the Gutzwiller approximation from quantum mechanics to the Brownian case. In Sec. IV we present results obtained using the adapted Gutzwiller approximation for the steady-state drift and on-site number fluctuations of the Brownian system. In particular, we explore the full range of interaction strengths from noninteracting to strongly interacting particles in the case of on-site and nearest-neighbor interactions. In Sec. V we summarize the results and comment on possible extensions and future uses of these methods.

II. MANY-BODY FORMULATION OF BROWNIAN MOTION

In this section we briefly review the creation and annihilation operator formalism for classical particles [17,18] and the many-body master equation for interacting Brownian particles [9]. In the operator formalism for indistinguishable classical particles [17,18], the state of the system, $|P(t)\rangle$, evolves in time via

$$\frac{d|P(t)\rangle}{dt} = \hat{\mathcal{L}}|P(t)\rangle, \tag{1}$$

where $\hat{\mathcal{L}}$ is the evolution operator, which we assume to be time independent. We further assume that a zeroth eigenvalue of $\hat{\mathcal{L}}$ exists, $\hat{\mathcal{L}}|P_0\rangle = 0$, such that the system has a steady state given by $|P_0\rangle$.

For out-of-equilibrium systems, $\hat{\mathcal{L}}$ is not self-adjoint: $\hat{\mathcal{L}} \neq \hat{\mathcal{L}}^\dagger$. As a result, the left and right eigenstates of $\hat{\mathcal{L}}$ do not have a simple relationship with each other [17]. The left eigenstate of the evolution operator corresponding to the zeroth eigenvalue is given by

$$\langle Q_0|\hat{\mathcal{L}} = 0. \tag{2}$$

Using the state $\langle Q_0|$, we can define the normalization condition

$$\langle Q_0|P(t)\rangle = 1 \tag{3}$$

and the average of an operator $\hat{O}$ as [17]

$$\langle \hat{O}\rangle(t) \equiv \langle Q_0|\hat{O}|P(t)\rangle. \tag{4}$$

Here, we are most interested in the average of an operator in the nonequilibrium steady state

$$\langle \hat{O}\rangle_{\text{ss}} \equiv \langle Q_0|\hat{O}|P_0\rangle. \tag{5}$$

The non-self-adjoint nature of the evolution operator and the definition of the average via Eq. (4) are the key differences between this formalism and quantum mechanics [17].

A many-body master equation describing discrete hopping on a deep-well periodic potential has been formulated in terms of bosonic creation ($\hat{a}_i^\dagger$) and annihilation ($\hat{a}_i$) operators [9]. Similar to quantum mechanics, these operators

describe the creation and annihilation of a Brownian particle in well (or site) i of the potential and satisfy the usual bosonic commutation relations $[\hat{a}_i, \hat{a}_j^\dagger] = \delta_{ij}$. The creation and annihilation operators act on the number state for the ith site $|n\rangle_i$ in the following way: $\hat{a}_i^\dagger|n\rangle_i = \sqrt{n+1}|n+1\rangle_i$ and $\hat{a}_i|n\rangle_i = \sqrt{n}|n-1\rangle_i$. The interaction between particles in the many-body master equation arises from a top-hat interaction potential [9]. The hopping rates in the many-body master equation are a function of the occupation number of the departure and arrival sites. In the case of nearest-neighbor interactions, the many-body master equation describes a particular type of misanthrope process [15]. In this paper we only consider the case of nearest-neighbor interactions. The evolution operator for the many-body master equation is given by

$$\hat{\mathcal{L}} = \sum_i [\hat{a}_{i+1}^\dagger \hat{\kappa}_i^+ \hat{a}_i + \hat{a}_{i-1}^\dagger \hat{\kappa}_i^- \hat{a}_i - \hat{a}_i^\dagger(\hat{\kappa}_i^+ + \hat{\kappa}_i^-)\hat{a}_i], \tag{6}$$

where $\hat{\kappa}_i^+$ and $\hat{\kappa}_i^-$ are the (number-dependent) forward and backward hopping rates, respectively. For a short-range top-hat potential, the hopping rates are well approximated by [9]

$$\hat{\kappa}_i^+ \approx \kappa_i^+ e^{-\beta_i \hat{n}_{i+1} + \alpha_i \hat{n}_i}, \tag{7}$$

$$\hat{\kappa}_i^- \approx \kappa_i^- e^{-\beta_i \hat{n}_{i-1} + \alpha_i \hat{n}_i}, \tag{8}$$

where $\hat{n}_i = \hat{a}_i^\dagger \hat{a}_i$ is the number operator acting on site i and $\kappa_i^\pm$ are the hopping rates for a single particle, which, in the deep-well limit, are given by Kramers rate. The parameters $\alpha_i > 0$ raise the bottom of the wells of the effective many-body potential. This lowers the energy barrier between sites, which increases the hopping rate. Therefore the α_i terms can be interpreted as a dimensionless quantity representing the strength of the repulsive on-site interaction between particles. The $\beta_i > 0$ terms raise the barrier height between adjacent wells of the effective many-body potential if the wells are occupied. This decreases the hopping rate of a particle between adjacent wells. Therefore the β_i terms can be interpreted as a dimensionless quantity representing the strength of the repulsive nearest-neighbor interaction. The master equation (1) with time evolution operator (6) has been shown to be equivalent to a next-neighbor misanthrope process and the ASEP and ZRP in various limits in Refs. [9,24].

Here we consider N particles spread across an M-well periodic system where we are interested in the nonequilibrium steady-state drift and on-site number fluctuations. It has been shown [9] that, in this case, it suffices to use the reduced evolution operator for a single period, given by

$$\hat{\mathcal{L}}_R = \sum_{i=1}^M [\hat{a}_{i+1}^\dagger \hat{\kappa}_i^+ \hat{a}_i + \hat{a}_{i-1}^\dagger \hat{\kappa}_i^- \hat{a}_i - \hat{a}_i^\dagger(\hat{\kappa}_i^+ + \hat{\kappa}_i^-)\hat{a}_i], \tag{9}$$

with periodic boundary conditions. A continuity equation for the number of particles at a single site can be obtained using the "Heisenberg" equations of motion [9]

$$\frac{d\hat{n}_i}{dt} = -(\hat{j}_i - \hat{j}_{i-1}), \tag{10}$$

where $\hat{j}_i = \hat{a}_{i+1}^\dagger \hat{\kappa}_i^+ \hat{a}_i - \hat{a}_i^\dagger \hat{\kappa}_{i+1}^- \hat{a}_{i+1}$ is the current operator.

From the continuity equation, we can derive an equation for the nonequilibrium steady-state drift as [9]

$$v = \frac{L}{N} \sum_{i=1}^{M} \langle \hat{j}_i \rangle_{\text{ss}}, \tag{11}$$

where L is the period of the potential. Another interesting parameter for Brownian particle systems is the steady-state on-site number fluctuations given by

$$\Delta n_i \equiv \langle \hat{n}_i^2 \rangle_{\text{ss}} - \langle \hat{n}_i \rangle_{\text{ss}}^2. \tag{12}$$

Due to the nonlinear nature of $\hat{\mathcal{L}}_R$, the steady state $|P_0\rangle$, defined by $\hat{\mathcal{L}}_R|P_0\rangle = 0$, cannot be determined analytically in general. In Ref. [9] the limiting cases of weak and strong interactions have been considered, but it is of interest to be able to explore the transition from noninteracting to strongly interacting particles. It is possible to solve for the ground state of $\hat{\mathcal{L}}_R$ numerically. However, for N particles across M lattice sites, the number of possible configurations grows as $(N + M - 1)!/[N!(M - 1)!]$, and thus numerical solutions are only possible for small systems. Approximation methods are necessary for larger systems. An approach to this is introduced in the next section.

III. GUTZWILLER APPROXIMATION FOR BROWNIAN PARTICLES

The Bose-Hubbard model [19] represents an analogous many-body quantum system to the many-body Brownian master equation. The Gutzwiller approximation has been applied to treating the transition from weak to strong interactions of the Bose-Hubbard model [22,25,26] and is thus a promising approach for the Brownian case. In quantum mechanics the Gutzwiller approximation factorizes the ground-state wave function as a product of single-site wave functions [22,25]. This neglects correlations between sites and has been shown to be equivalent to decoupling mean-field treatments [27]. In the quantum case, the ground-state single-site wave functions can be solved by evolving an arbitrary initial state forward in imaginary time until it converges [26], or by using variational approaches [21]. The Gutzwiller approximation is a numerically efficient method to obtain the ground state for large systems [26].

In the operator formalism for classical particles, analogous to the Gutzwiller approximation for the Bose-Hubbard model, the steady state is approximated as

$$|P_0\rangle = \prod_{i=1}^{M} |\phi_0\rangle_i, \tag{13}$$

where $|\phi_0\rangle_i$ is the state for site i. The state for a single site is expanded in terms of the number states n, as

$$|\phi_0\rangle_i = \sum_{n=0}^{\infty} c_i^n |n\rangle_i, \tag{14}$$

where the coefficient c_i^n is related to the probability, p_i^n, of n particles occupying site i by $p_i^n = (\rho^n/n!)^{1/2} c_i^n$ (see Appendix A). Analogous to the quantum case, the unknown coefficients c_i^n can be determined by an iterative procedure that we will describe in Sec. III B.

A similar approach has been applied previously to classical interacting particle systems where is it known the exact steady state has a factorized form, such as the ZRP [28]. In general the steady state will not have a factorized form; however, it is often a good approximation in the large-system limit. Assuming a factorized form of the steady state is sometimes referred to as a product-measure ansatz [28,29]. In this paper, we refer to this as the Gutzwiller approximation because, in the operator formalism, the factorized steady state is identical to the Gutzwiller approximation of quantum mechanics, and we solve for this steady state using methods that are analogous to those in the quantum case.

In the operator formalism for classical particles, the left eigenstate is not the adjoint of the right eigenstate, so we also need to approximate the left eigenstate as a product of single-site states

$$\langle Q_0| = \prod_{i=1}^{M} \langle q_0|_i. \tag{15}$$

An effective single-site evolution operator is found by averaging over the operators acting on neighboring sites

$$\hat{\mathcal{L}}_i^{\text{eff}} = \prod_{m \neq i} \langle q_0|_m \hat{\mathcal{L}}_R \prod_{m' \neq i} |\phi_0\rangle_{m'}. \tag{16}$$

For simplicity, for the remainder of this paper, we consider the uniform case where $\alpha_i = \alpha$, $\beta_i = \beta$, and $\kappa_i^{\pm} = \kappa_{\pm}$. In this case, in the steady state, each site is in an identical state. Under these assumptions we derive the effective evolution operator for site i of the form

$$\hat{\mathcal{L}}_i^{\text{eff}} = (\kappa_+ + \kappa_-)(\gamma_1' e^{\alpha \hat{n}_i} \hat{a}_i - \gamma_1 \hat{a}_i^{\dagger} e^{\alpha \hat{n}_i} \hat{a}_i)$$
$$+ (\kappa_+ + \kappa_-)(\gamma_2 \hat{a}_i^{\dagger} e^{-\beta \hat{n}_i} - \gamma_2' e^{-\beta \hat{n}_i}), \tag{17}$$

where we have introduced the parameters

$$\gamma_1 = \langle q_0|_m e^{-\beta \hat{n}_m} |\phi_0\rangle_m, \tag{18}$$

$$\gamma_1' = \langle q_0|_m \hat{a}_m^{\dagger} e^{-\beta \hat{n}_m} |\phi_0\rangle_m, \tag{19}$$

$$\gamma_2 = \langle q_0|_m e^{\alpha \hat{n}_m} \hat{a}_m |\phi_0\rangle_m, \tag{20}$$

$$\gamma_2' = \langle q_0|_m \hat{a}_m^{\dagger} e^{\alpha \hat{n}_m} \hat{a}_m |\phi_0\rangle_m. \tag{21}$$

The ith state $|\phi_0\rangle_i$ then satisfies $\hat{\mathcal{L}}_i^{\text{eff}}|\phi_0\rangle_i = 0$. We will demonstrate a method of self-consistently solving this nonlinear equation in Sec. III B below. We also require that the left eigenstate satisfies $\langle q_0|_i \hat{\mathcal{L}}_i^{\text{eff}} = 0$. This last requirement is satisfied by taking the left eigenstate to be the coherent state

$$\langle q_0|_i = \langle 0| e^{\sqrt{\rho} \hat{a}_i}, \tag{22}$$

where $\rho = N/M$ is the steady-state density of particles. Note that $\hat{\mathcal{L}}_R$ [Eq. (9)] conserves particle number and thus $\langle Q_0|$, where $\langle Q_0|\hat{\mathcal{L}}_R = 0$, must have a fixed number. However, under the Gutzwiller approximation, $\langle q_0|_i$ cannot have a fixed number of particles due to particle hopping between sites, and Eq. (22) allows for these number fluctuations.

From Eq. (22) it follows that $\langle q_0|_i$ is the left eigenstate of the creation operator: $\langle q_0|_i \hat{a}_i^{\dagger} = \sqrt{\rho} \langle q_0|_i$. Therefore the parameters γ_1' and γ_2' simplify to $\gamma_1' = \sqrt{\rho} \gamma_1$ and $\gamma_2' = \sqrt{\rho} \gamma_2$. The effective single-site evolution operator (17) simplifies to

$$\hat{\mathcal{L}}_i^{\text{eff}} = (\kappa_+ + \kappa_-)(\sqrt{\rho} - \hat{a}_i^{\dagger})(\gamma_1 e^{\alpha \hat{n}_i} \hat{a}_i - \gamma_2 e^{-\beta \hat{n}_i}). \tag{23}$$

From this form of the evolution operator it is easy to see that $\langle q_0|_i \hat{\mathcal{L}}_i^{\text{eff}} = 0$ with $\langle q_0|_i$ given by Eq. (22).

Using the Gutzwiller approximation of the left and right states in Eqs. (13) and (15), it follows that the steady-state average of an operator of the form $\hat{O} = \prod_j \hat{o}_j$ is

$$\langle Q_0|\hat{O}|P_0\rangle = \prod_{i=1}^M \langle q_0|_i \hat{o}_i|\phi_0\rangle_i. \tag{24}$$

Using the Gutzwiller approximation, the expression for the drift per particle in Eq. (11) becomes

$$v = \frac{L}{N}\sum_{i=1}^M [\kappa_i^+ \langle q_0|_{i+1}\hat{a}_{i+1}^\dagger e^{-\beta_i\hat{n}_{i+1}}|\phi_0\rangle_{i+1}\langle q_0|_i e^{\alpha_i\hat{n}_i}\hat{a}_i|\phi_0\rangle_i$$
$$- \kappa_i^- \langle q_0|_{i-1}\hat{a}_{i-1}^\dagger e^{-\beta_i\hat{n}_{i-1}}|\phi_0\rangle_{i-1}\langle q_0|_i e^{\alpha_i\hat{n}_i}\hat{a}_i|\phi_0\rangle_i]. \tag{25}$$

In the uniform case, under the above simplifying assumptions, this can be written as

$$v = v_0 \frac{\gamma_1\gamma_2}{\sqrt{\rho}}, \tag{26}$$

where v_0 is the single-particle drift given by $L(\kappa_+ - \kappa_-)$ [9]. Similarly, the steady-state on-site number fluctuations are given by

$$\Delta n_i = \langle q_0|_i \hat{n}_i^2|\phi_0\rangle_i - \langle q_0|_i \hat{n}_i|\phi_0\rangle_i^2 \tag{27}$$
$$= \rho\langle q_0|_i \hat{a}_i^2|\phi_0\rangle_i + \sqrt{\rho}\langle q_0|_i \hat{a}_i|\phi_0\rangle_i - \rho\langle q_0|_i \hat{a}_i|\phi_0\rangle_i^2. \tag{28}$$

A. Comparison with mean-field approaches

It has been shown that applying the Gutzwiller approximation to the Bose-Hubbard model gives similar results to decoupling mean-field approaches [27]. A similar result also holds for the Brownian case. Let us assume that the state of the system can be factorized as Eq. (13) for all time, i.e.,

$$|P(t)\rangle = \prod_{i=1}^M |\phi(t)\rangle_i, \tag{29}$$

and that Eqs. (15) and (22) also hold. Taking the average of the continuity equation, Eq. (10), with these assumptions we arrive at

$$\frac{d\rho_i}{dt} = \kappa_+\sqrt{\rho}(\langle e^{-\beta\hat{n}_i}\rangle\langle e^{\alpha\hat{n}_{i-1}}\hat{a}_{i-1}\rangle - \langle e^{-\beta\hat{n}_{i+1}}\rangle\langle e^{\alpha\hat{n}_i}\hat{a}_i\rangle)$$
$$+ \kappa_-\sqrt{\rho}(\langle e^{-\beta\hat{n}_i}\rangle\langle e^{\alpha\hat{n}_{i+1}}\hat{a}_{i+1}\rangle - \langle e^{-\beta\hat{n}_{i-1}}\rangle\langle e^{\alpha\hat{n}_i}\hat{a}_i\rangle), \tag{30}$$

where we have used $\rho_i = \langle\hat{n}_i\rangle$ and $\langle\hat{a}_i\rangle = \rho_i/\sqrt{\rho}$. The last relation results from $\rho_i = \langle\hat{n}_i\rangle = \langle\hat{a}_i^\dagger\hat{a}_i\rangle = \sqrt{\rho}\langle\hat{a}_i\rangle$, which follows from Eq. (22).

In the noninteracting limit ($\beta = \alpha = 0$), we find

$$\frac{d\rho_i}{dt} = \kappa_-\rho_{i+1} + \kappa_+\rho_{i-1} - \kappa_+\rho_i - \kappa_-\rho_i \tag{31}$$

as expected. In the limit where $\beta \gg 1$, $\alpha = 0$, and there is at most one particle per site, the many-body master equation reduces to the ASEP. For $\beta \gg 1$, the term $e^{-\beta\hat{n}_i}$ is zero if site i is occupied. Therefore the average $\langle e^{-\beta\hat{n}_i}\rangle$ is the probability of zero particles on site i: $\langle e^{-\beta\hat{n}_i}\rangle = 1 - \rho_i$. In this limit, Eq. (30)

reduces to

$$\frac{d\rho_i}{dt} = -\kappa_+\rho_i(1 - \rho_{i+1}) + \kappa_-\rho_{i+1}(1 - \rho_i)$$
$$+ \kappa_+\rho_{i-1}(1 - \rho_i) - \kappa_-\rho_i(1 - \rho_{i-1}). \tag{32}$$

This is the same result found using mean-field treatments of the ASEP [30]. Equations (31) and (32) thus provide a connection between the Gutzwiller method and mean-field approaches.

B. Self-consistent numerical method

In this section we illustrate a numerical method to self-consistently solve for $|\phi_0\rangle_i$, i.e., solve for the coefficients c_n^i in Eq. (14). Let us assume a *time-dependent* evolution operator of the form

$$\hat{\mathcal{L}}_i^{\text{eff}}(t) = (\kappa_+ + \kappa_-)(\sqrt{\rho} - \hat{a}_i^\dagger)[\gamma_1(t)e^{\alpha\hat{n}_i}\hat{a}_i - \gamma_2(t)e^{-\beta\hat{n}_i}], \tag{33}$$

where we have defined the time-dependent quantities

$$\gamma_1(t) = \langle q_0|_i e^{-\beta\hat{n}_i}|\phi(t)\rangle_i, \tag{34}$$

$$\gamma_2(t) = \langle q_0|_i e^{\alpha\hat{n}_i}\hat{a}_i|\phi(t)\rangle_i. \tag{35}$$

In principle, we can determine the steady state $|\phi_0\rangle_i$ by evolving an arbitrary initial state forward in time via Eq. (33) evaluating the parameters $\gamma_1(t)$ and $\gamma_2(t)$ at each time. Mathematically, we have

$$|\phi_0\rangle_i = \lim_{t\to\infty}|\phi(t)\rangle_i = \mathcal{T}\lim_{t\to\infty}\exp\left\{\int_0^t ds\hat{\mathcal{L}}_i^{\text{eff}}(s)\right\}|\phi(0)\rangle_i, \tag{36}$$

where $\mathcal{T}$ is the time-ordering operator.

A numerical algorithm to implement this process in discrete time is as follows. An initial state is chosen such that it gives the density $\langle q_0|_i\hat{n}_i|\phi^{(1)}\rangle_i = \rho$. Using the effective evolution operator (33), the state is propagated forward in time by

$$|\tilde{\phi}^{(j+1)}\rangle_i = \exp\left[\Delta t\hat{\mathcal{L}}_i^{\text{eff}}\left(\gamma_1^{(j)}, \gamma_2^{(j)}\right)\right]|\phi^{(j)}\rangle_i, \tag{37}$$

where j is the number of iterations, Δt is a sufficiently small time step (i.e., smaller than the inverse of the largest entry in the evolution operator), and $|\tilde{\phi}^{(j+1)}\rangle_i$ is an un-normalized state. The state is normalized by

$$|\phi^{(j+1)}\rangle_i = \frac{|\tilde{\phi}^{(j+1)}\rangle_i}{\langle q_0|\tilde{\phi}^{(j+1)}\rangle_i}, \tag{38}$$

such that $\langle q_0|\phi^{(j+1)}\rangle_i = 1$.

For each iteration, the parameters $\gamma_1^{(j)}$ and $\gamma_2^{(j)}$ are evaluated using the state $|\phi^{(j)}\rangle_i$. The state $|\phi^{(j)}\rangle_i$ is self-consistently evolved forward according to Eq. (37) until it converges to a steady state. The convergence criterion used in this paper is

$$\left|1 - \frac{\gamma_2^{(j)}}{\gamma_2^{(j+1)}}\right| < \epsilon, \tag{39}$$

where $\epsilon \ll 1$ is the convergence threshold. In the simulations in this paper, $\epsilon = 10^{-10}$. This self-consistent approach only requires us to evaluate the state at a single site and therefore provides an efficient numerical method to obtain results for

large systems. Once we have found the steady state, we can use Eqs. (26) and (27) to evaluate quantities of interest.

IV. NUMERICAL RESULTS

In this section we present results obtained using the adapted Gutzwiller approximation. First we consider the cases where $\alpha = 0$ and $\beta = 0$ separately, before considering the more general case where $\alpha \neq 0$ and $\beta \neq 0$. Finally, we compare the system behavior with the behavior of the quantum Bose-Hubbard model.

A. $\alpha = 0$ case

When $\alpha = 0$ and $\beta > 0$, there is a repulsive interaction between particles in the ith site and neighboring ($i \pm 1$) sites. The weakly interacting ($\beta \ll 1$) and strongly interacting ($\beta \gg 1$) regimes of the many-body master equation have been explored analytically in Ref. [9]. We begin by comparing the Gutzwiller method with these results.

For $\rho < 1$, in the limit $\beta \gg 1$, the many-body master equation reduces to an operator formulation of the ASEP [9]. Analytical expressions for the ASEP drift and number fluctuations are [9]

$$v = v_0 \frac{(1 - \rho)}{(1 - 1/M)}, \tag{40}$$

$$\Delta n_i = \rho(1 - \rho). \tag{41}$$

In addition, a Bogoliubov method has been used to obtain analytical expressions in the weakly interacting regime ($\beta \ll 1$, $\alpha \ll 1$) in the limit of a large number of particles ($N \gg 1$). Analytical expressions for the steady-state drift per particle and the number fluctuations in this limit are given by [9]

$$v = v_0 + v_0 \rho(\alpha - \beta), \tag{42}$$

$$\Delta n_i = \rho[1 - \rho(\alpha + \beta)]. \tag{43}$$

Figure 1 shows a comparison between the Gutzwiller results and these two limiting cases. The results obtained via the Gutzwiller approximation not only agree well with the analytical expressions in both limits, but also provide values for the transition between these limits.

For small system sizes, it is possible to find the exact steady state $|P_0\rangle$, where $\hat{\mathcal{L}}_R|P_0\rangle = 0$, numerically. We next compare the Gutzwiller results at a fixed density with exact numerical calculations at the same density $\rho = N/M$ but different numbers of sites. Figure 2 shows the drift and number fluctuations in the case where $\alpha = 0$. In this case, both the drift and number fluctuations decrease with increasing interaction strength. Figure 2 also shows that the exact numerical calculations for the drift (number fluctuations) decrease (increase) as M increases, with the Gutzwiller results representing a lower (upper) bound. Unfortunately, we are not able to treat larger system sizes using the exact approach; however, these results align with our expectation that the Gutzwiller approximation corresponds to the large-system limit ($M \gg 1$ and $N \gg 1$).

Using the Gutzwiller approximation, we can explore the behavior of the drift and number fluctuations for a range of densities and interaction strengths. In Fig. 3, we show plots of the steady-state drift and number fluctuations as a function of
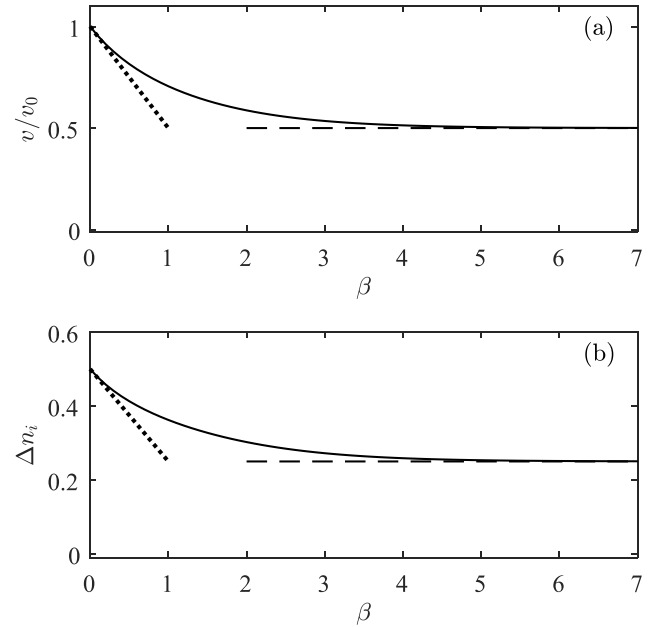

FIG. 1. Plots of (a) steady-state drift and (b) on-site number fluctuations obtained via the Gutzwiller approximation (solid line). For comparison, results obtained from a Bogoliubov method [Eqs. (42) and (43)] (dotted line) and results from the ASEP [Eqs. (40) and (41)] (dashed line) in the $M \gg 1$ limit are also shown. Parameters used are $\kappa_+/\kappa_- = 1.2$, $\rho = 0.5$, $L = 1$, and $\alpha = 0$.

β with $\alpha = 0$. In this case, the steady-state drift and number fluctuations decay exponentially to asymptotic values with increasing interaction strength. For $\rho \geqslant 1$ the drift decays to zero for large interaction strengths but tends to a finite value for $\rho < 1$. The number fluctuations only decay to zero in the large-interaction limit if ρ is an integer. These results will be explored in more detail below. The large-interaction limit with densities greater than 1 is often referred to as the asymmetric simple k-exclusion process [31].

In Fig. 4, we show a contour plot of the drift and on-site number fluctuations as a function of density and β for $\alpha = 0$. Figure 5 shows more details of how the drift and number fluctuations vary with ρ for specific values of β.

In Figs. 4(a) and 5(a) we see that for $\rho > 1$ the drift tends to zero for large β. The drift also approaches zero faster for larger densities. For $\rho > 1$ the neighboring site will be occupied. This means that when $\beta \gg 1$, the hopping rates given by Eqs. (7) and (8) will be very small resulting in approximately zero drift.

Figures 4(b) and 5(b) show the behavior of the number fluctuations as a function of β and ρ. The general trend is for the fluctuations to increase with density. However, in the limit $\beta \gg 1$, the number fluctuations go to zero for integer densities. These integer values of density also have a strong influence on the number fluctuations for densities close to these values, creating "fingers" of density with reduced fluctuations. Note that despite the drift going to zero for $\rho \geqslant 1$ in the $\beta \gg 1$ limit, the on-site number fluctuations are in general nonzero except at integer densities.

To understand the number fluctuations further, we compare the number state distribution p_i^n [see Eqs. (14) and (A9)] for
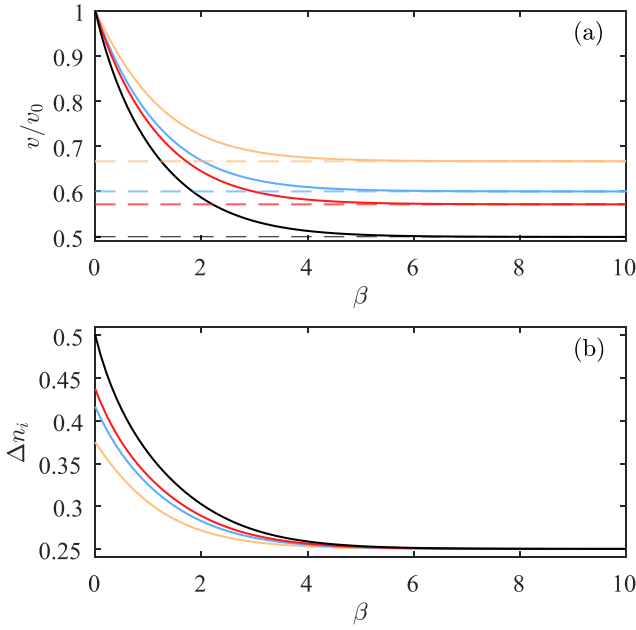
FIG. 2. Plots of results evaluated via the Gutzwiller approximation (solid black line) compared with results evaluated via an exact numerical method (solid colored lines). (a) shows the steady-state drift per particle, and (b) shows the steady-state on-site number fluctuations. In both cases these are plotted as a function of β for a lattice with a density of $\rho = 0.5$ and with $M = 4$ (yellow), $M = 6$ (blue), and $M = 8$ (red). Parameters used are $\kappa_+/\kappa_- = 1.2$, $L = 1$, and $\alpha = 0$. For (a) the dashed lines show the ASEP limit given by Eq. (40). The black dashed line shows the case where $M \to \infty$.

FIG. 4. Contour plots of (a) the steady-state bulk drift and (b) the number fluctuations calculated via the Gutzwiller approximation as a function of the density and the nearest-neighbor interaction strength β. The parameters used are $L = 1$, $\alpha = 0$, and $\kappa_+/\kappa_- = 1.2$.

an integer and noninteger density as the interaction strength increases. Figures 6(a)–6(c) show the case for a noninteger density, and Figs. 6(d)–6(f) show the case for an integer density. In the integer case, the state converges to a single number
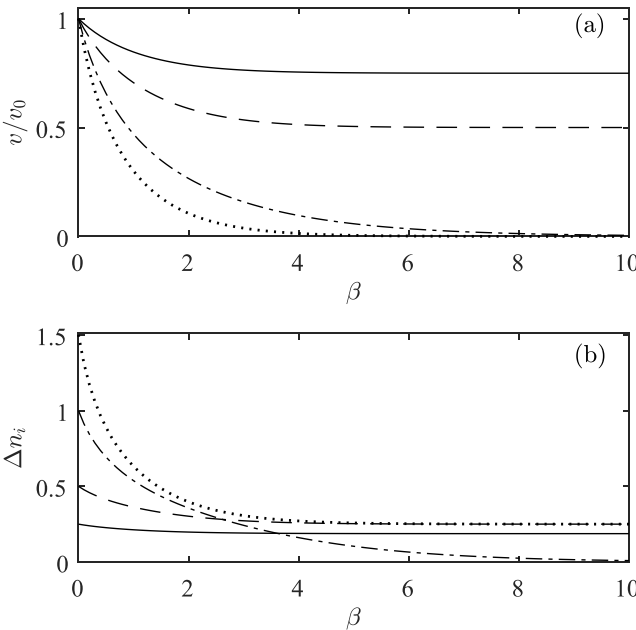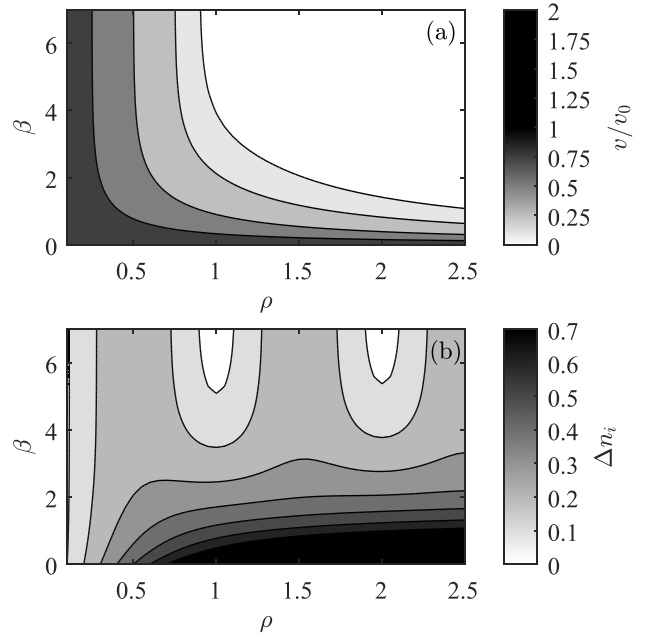

FIG. 3. Plots of (a) the steady-state drift per particle and (b) the number fluctuations calculated via the Gutzwiller approximation for systems with various densities. In all cases, $\alpha = 0$ and the different densities used are as follows: $\rho = 0.25$ (solid line), $\rho = 0.5$ (dashed line), $\rho = 1$ (dash-dotted line), and $\rho = 1.5$ (dotted line). The parameters used are $L = 1$ and $\kappa_+/\kappa_- = 1.2$.
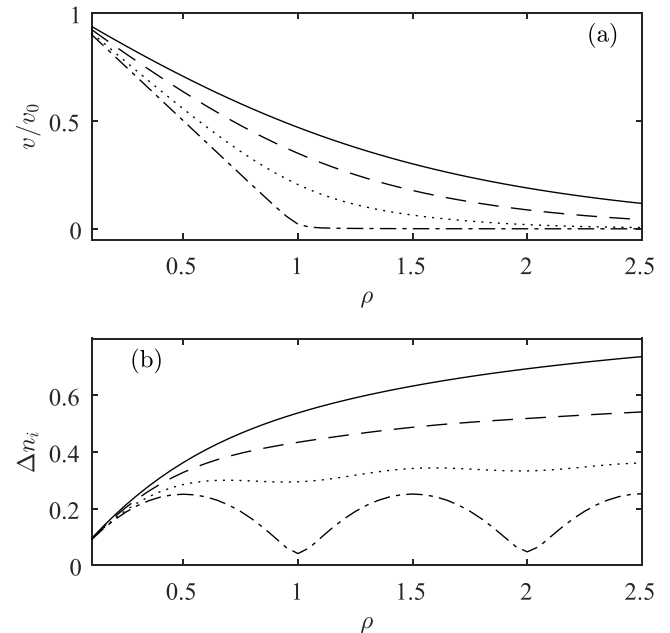

FIG. 5. Plots of (a) the steady-state drift per particle and (b) the number fluctuations calculated via the Gutzwiller approximation for systems with various densities. In all cases, $\alpha = 0$ and the different values for β used are as follows: $\beta = 1$ (solid line), $\beta = 1.5$ (dashed line), $\beta = 2.5$ (dotted line), and $\beta = 7$ (dash-dotted line). The parameters used are $L = 1$ and $\kappa_+/\kappa_- = 1.2$.
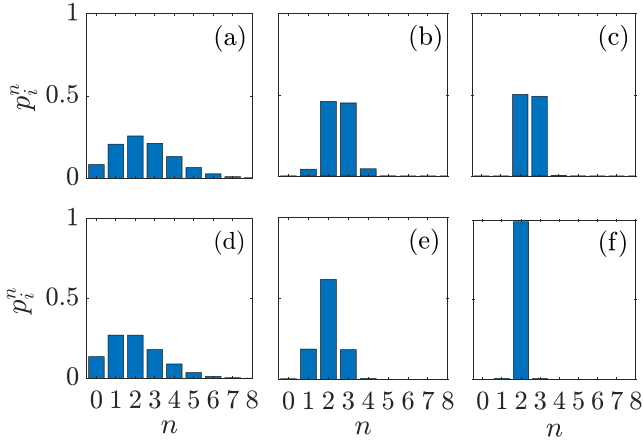
FIG. 6. Plots of the number state distribution calculated using the Gutzwiller approximation with various interaction strengths. In (a)–(c), $\rho = 2.5$, and in (d)–(f), $\rho = 2$. The values shown for β are (a) $\beta = 0$, (b) $\beta = 2$, (c) $\beta = 10$, (d) $\beta = 0$, (e) $\beta = 2$, and (f) $\beta = 10$. Parameters used are $\alpha = 0$ and $\kappa_+/\kappa_- = 1.2$.

state with increasing β. This results in the zero number fluctuations we observed in Fig. 4(b). In contrast, in the noninteger case, for large β the state of the system becomes a near-equal distribution of two number states, and as a result, the number fluctuations cannot be zero.

B. $\beta = 0$ case

In the case where $\beta = 0$ and $\alpha > 0$ in Eqs. (7) and (8), the repulsive interactions only occur between particles occupying the same lattice site, and the many-body master equation reduces to the ZRP. Let us first compare the Gutzwiller approximation at a specific density with exact numerical cal-
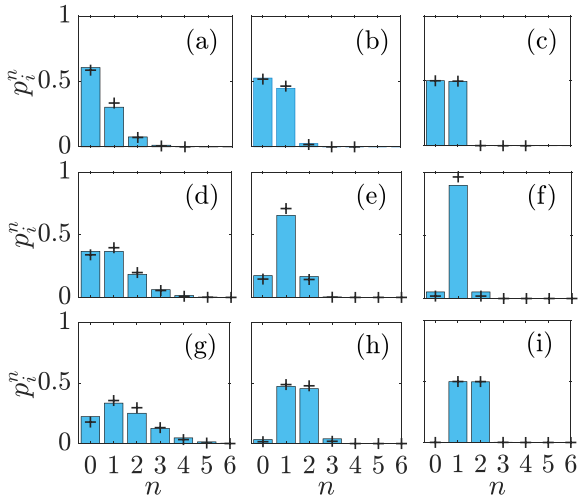

FIG. 7. Plots of the number state distribution for an arbitrary site calculated using the Gutzwiller approximation (bars) and the exact numerical method (crosses) with various interaction strengths. Density values shown are (a)–(c) $\rho = 0.5$ (exact: $M = 8$, $N = 4$), (d)–(f) $\rho = 1$ (exact: $M = 7$, $N = 7$), and (g)–(i) $\rho = 1.5$ (exact: $M = 6$, $N = 9$). Interaction strengths shown are $\alpha = 0$ [(a), (d), and (g)], $\alpha = 2$ [(b), (e), and (h)], and $\alpha = 5$ [(c), (f), and (i)]. Other parameters are $\beta = 0$ and $\kappa_+/\kappa_- = 1.2$.
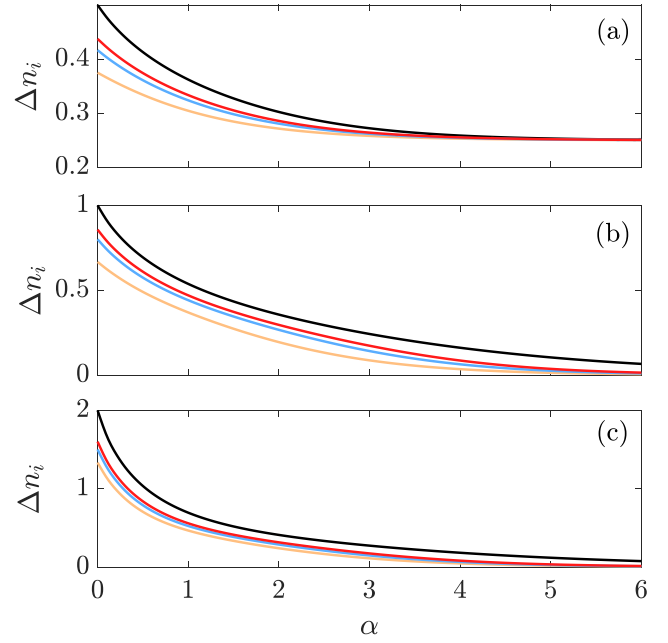

FIG. 8. Plots of the steady-state on-site number fluctuations evaluated via the Gutzwiller approximation (solid black line) compared with results evaluated via an exact numerical method (solid colored lines). The densities shown are (a) $\rho = 0.5$, (b) $\rho = 1$, and (c) $\rho = 2$. The system sizes used for the exact solutions in (a) are $M = 4$ (yellow), $M = 6$ (blue), and $M = 8$ (red), in (b) are $M = 3$ (yellow), $M = 5$ (blue), and $M = 7$ (red), and in (c) are $M = 3$ (yellow), $M = 4$ (blue), and $M = 5$ (red). Parameters are $\kappa_+/\kappa_- = 1.2$, $L = 1$, and $\beta = 0$.

culations at the same density. Figure 7 shows the number state distribution for three different densities and three different interaction strengths. The results show a smoothly increasing suppression of the number fluctuations with increasing α, very similar to the case considered in Sec. IV B for increasing β and $\alpha = 0$. The Gutzwiller results display the same qualitative behavior as the exact solutions. Although not shown in this plot, agreement improves with increasing M (at the same density and α), consistent with the Gutzwiller results being the large-system limit.

The number fluctuations calculated via the two methods provide a more quantitative comparison (see Fig. 8). In line with the discussion in Sec. IV A, for integer values of density the number fluctuations tend to zero with large α, whereas, for $\rho = 0.5$, they tend to a finite value. Figure 8 shows that the exact solutions for the number fluctuations (at the same density and α) increase with increasing M, with the Gutzwiller results providing an upper bound.

Although the number fluctuations are exponentially suppressed with increasing $\alpha > 0$, the coupling rate has an exponential dependence on number [see Eqs. (7) and (8)] which reverses this effect leading to the possibility of large drifts. Figure 9 shows the drift for three different densities corresponding to the parameters in Fig. 8. There are three different regimes of behavior corresponding to the cases $\rho < 1$, $\rho = 1$, and $\rho > 1$ shown in Figs. 9(a), 9(b), and 9(c). When $\rho < 1$, the drift calculated via the exact numerical approach tends to a finite value for large α. The exact results show that the drift (at the same density and α) increases with increas-
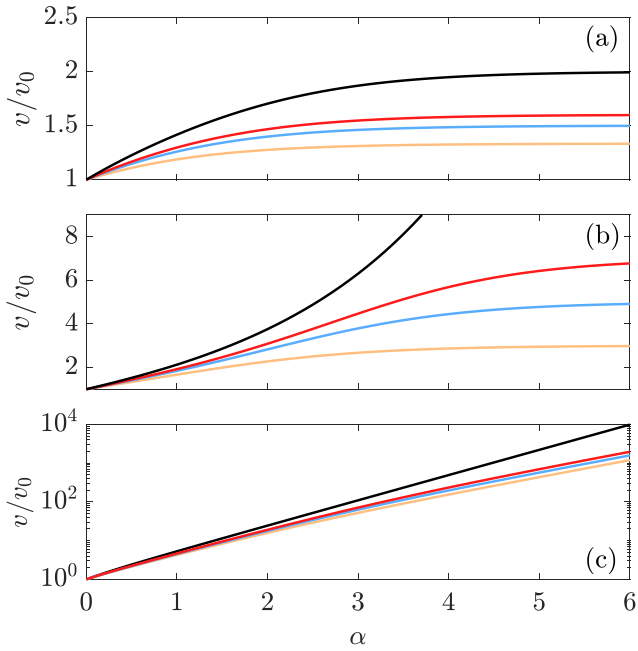
FIG. 9. Plots of the steady-state drift per particle evaluated via the Gutzwiller approximation (solid black line) compared with results evaluated via an exact numerical method (solid colored lines). The densities shown are (a) $\rho = 0.5$, (b) $\rho = 1$, and (c) $\rho = 2$. Note that in (c) the y axis has a logarithmic scale. The system sizes used for the exact solutions in (a) are $M = 4$ (yellow), $M = 6$ (blue), and $M = 8$ (red), in (b) are $M = 3$ (yellow), $M = 5$ (blue), and $M = 7$ (red), and in (c) are $M = 3$ (yellow), $M = 4$ (blue), and $M = 5$ (red). Other parameters are $\kappa_+/\kappa_- = 1.2$, $L = 1$, and $\beta = 0$.

ing M, again with the Gutzwiller results providing an upper bound. For $\rho = 1$, the exact results tend to a finite value given by

$$\frac{v}{v_0} = M \tag{44}$$

for large α. In this case, unlike the exact solution, the Gutzwiller solution diverges for large α. However, within the confines of the discrete master equation model (more on this below), this result is consistent with the Gutzwiller approximation being the large-system limit, as Eq. (44) will tend to infinity in this case. For $\rho > 1$ the exact solution grows exponentially with α. The exponential growth rate also increases with M, with the Gutzwiller approximation providing an upper bound. Although not shown, the Gutzwiller approach also agrees with the Bogoliubov results (42) and (43) in the $\alpha \ll 1$ limit. While the number fluctuation (see Fig. 8) and number distribution (see Fig. 7) results are consistent with the interpretation that the Gutzwiller approximation represents the large-system limit, due to small differences in the state leading to large changes in the drift, away from the $\alpha \ll 1$ limit the Gutzwiller approximation does not reproduce the trends seen in the drift from exact numerical solutions (see Fig. 9) for any values of ρ for the small numbers of sites we have been able to simulate.

We can understand the physical origin of the $\rho \geqslant 1$ drift behavior of the master equation by considering the original top-hat potential. Increasing α with $\rho \geqslant 1$ raises the bot-
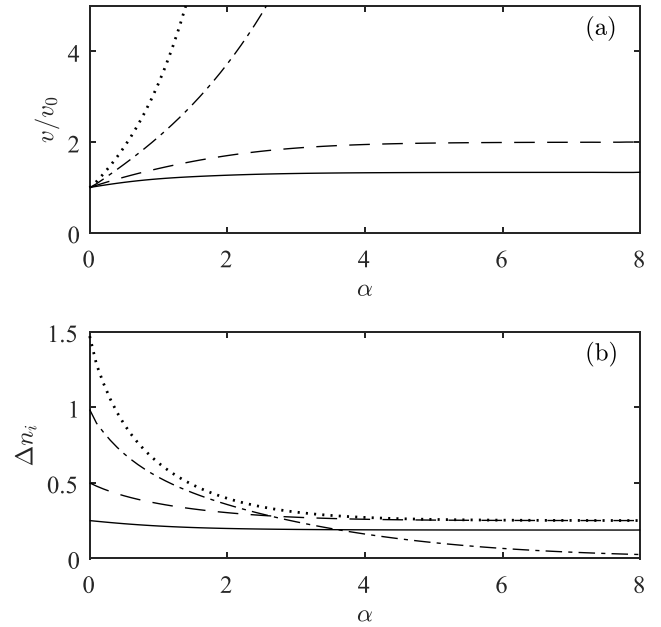

FIG. 10. Plots of (a) the steady-state drift per particle and (b) the number fluctuations calculated via the Gutzwiller approximation for systems with various densities. In all cases, $\beta = 0$ and the different densities used are as follows: $\rho = 0.25$ (solid line), $\rho = 0.5$ (dashed line), $\rho = 1$ (dash-dotted line), and $\rho = 1.5$ (dotted line). The parameters used are $\kappa_+/\kappa_- = 1.2$ and $L = 1$.

tom of the potential well, effectively lowering the barrier to hopping and leading to an increased drift. It is, of course, not physically possible for the drift to keep increasing with interaction strength, and at some point the wells will become so shallow that the discrete master equation is no longer a valid description [9]. Thus the physics of the diverging drift in Fig. 9 is of no interest as some other physical phenomena will take over once α is large enough. Determining the point at which the discrete master equation breaks down (and the behavior beyond this point) is beyond the present master equation treatment.

In Fig. 10 we summarize results obtained using the Gutzwiller approximation for the ZRP for easy comparison with the $\beta = 0$ case from Sec. IV B. Figure 10(a) shows that the steady-state drift per particle increases from the noninteracting drift as the on-site interaction strength α increases. For $\rho < 1$, the drift approaches a finite value in the limit $\alpha \gg 1$. For $\rho \geqslant 1$, the drift increases exponentially with interaction strength. The steady-state number fluctuations, shown in Fig. 10(b), decrease as the interaction strength increases. This holds for all values of the density despite the fact that the drift increases with α in some cases. In fact, the number fluctuations have the same behavior with increasing α ($\beta = 0$) as they have with increasing β ($\alpha = 0$) [see Fig. 3(b)]. This behavior will be explored further below.

C. General case: $\alpha \neq 0$ and $\beta \neq 0$

More generally, α and β will both be nonzero. Let us first consider the number fluctuations. Comparing Figs. 3(b) and 10(b), one can see that the number fluctuations have the same dependence on α as on β. In fact, it is possible to show

that for a fixed density the Gutzwiller state depends only on the sum of these two parameters, $\alpha + \beta$ (see Appendix), and thus they have the same impact on the number fluctuations. One consequence of this is that the number state distribution shown in Fig. 6 and the plots in Figs. 4(b) and 5(b) hold with the replacement $\beta \rightarrow \alpha$.

The drift's dependence on α and β is more complicated. As an example, although the number fluctuations in Figs. 3(b) and 10(b) are the same, the corresponding drifts shown in Figs. 3(a) and 10(a) are very different.

As a further example, Fig. 11(a) shows the drift in the case $\alpha = \beta$. This demonstrates a zero gradient for small β [in agreement with Eq. (42)] and then an exponential decay to a finite value, except for the integer density case. In line with previous results in Secs. IV B and IV A, the drift goes to a finite value in the limit of large interactions for $\rho < 1$. However, unlike the $\alpha = 0$ case (cf. Fig. 3) the drift does not go to zero for $\beta \gg 1$ when $\rho > 1$, and unlike the $\beta = 0$ case (cf. Fig. 3) the drift does not diverge for $\alpha \gg 1$ when $\rho > 1$. This demonstrates the competition between these two interaction processes in the $\alpha \neq 0$ and $\beta \neq 0$ case.

To further understand the drift behavior in the $\rho \geqslant 1$ case, we plot the drift as a function of both α and β in Fig. 12. This shows that when $\alpha/\beta < 1$, we get the usual $\alpha = 0$ behavior where the drift decays exponentially to zero for increasing interaction strength. Similarly, when $\alpha/\beta > 1$, the drift increases exponentially with interaction strength. Only in the special case where $\alpha/\beta = 1$ does the drift tends to a finite (density dependent) value for large interaction strengths.

The density dependence of the drift in the $\alpha = \beta$ case is shown in Fig. 11(b). This shows suppressed drift close to integer values of density. This suppression becomes more pronounced as interaction strength increases. A simple calculation helps us to understand the origin of this behavior. In the limit where $\beta \gg 1$ and the density is $n \geqslant \rho \geqslant n + 1$, the number fluctuations of the Gutzwiller state are suppressed, and we can approximate the state by only two number states:

$$|\phi_0\rangle_i \approx c_i^n |n\rangle + c_i^{n+1} |n+1\rangle. \qquad (45)$$

The two unknown coefficients c_i^n and c_i^{n+1} can be determined from the normalization condition and the density. Details of these calculations are given in Appendix. The state (45) results in the number fluctuations

$$\Delta n_i = (\rho - n)(1 + n - \rho), \qquad (46)$$

which reflects the dash-dotted line shown in Fig. 5(b).

The state (45) also leads to a drift of the form

$$v = v_0 e^{-(\beta-\alpha)n} \frac{(1+n)}{\rho}(\rho - n)(1 + n - \rho). \qquad (47)$$

If $\beta \gg \alpha$, then we get the result

$$v = \begin{cases} 0, & n \geqslant 1 \\ v_0(1-\rho), & n = 0. \end{cases} \qquad (48)$$

This is consistent with the dash-dotted line shown in Fig. 5(a). However, if $\beta \sim \alpha$, then the on-site and nearest-neighbor interactions partially cancel, allowing hopping to occur for noninteger n. The case where $\alpha = \beta$ is shown in Fig. 11(b).
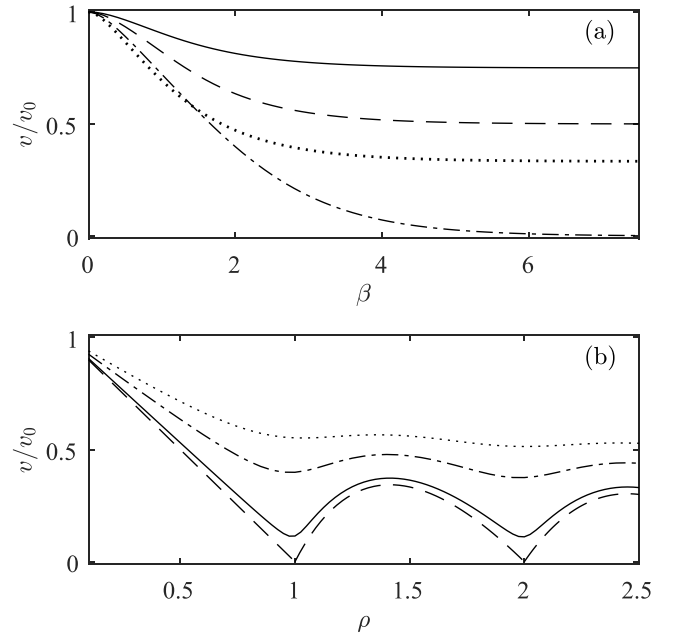

FIG. 11. Plots of the steady-state drift per particle evaluated via the Gutzwiller approximation with $\alpha = \beta$. In (a) the densities shown are as follows: $\rho = 0.25$ (solid line), $\rho = 0.5$ (dashed line), $\rho = 1$ (dash-dotted line), and $\rho = 1.5$ (dotted line). In (b) the values for β shown are as follows: $\beta = 1.5$ (dotted line), $\beta = 2$ (dash-dotted line), $\beta = 3.5$ (solid line), and $\beta = 10$ (dashed line). The parameters used are $L = 1$ and $\kappa_+/\kappa_- = 1.2$.

The numerical results show excellent agreement with Eq. (47) for $\beta \gtrsim 6$.

We can interpret these results as follows. Because $\beta \gg 1$ suppresses hopping between sites, the number fluctuations become zero for integer densities. However, due to the nonzero probability of occupying a second number state, they remain finite for noninteger densities. When $\beta \sim \alpha$, although number
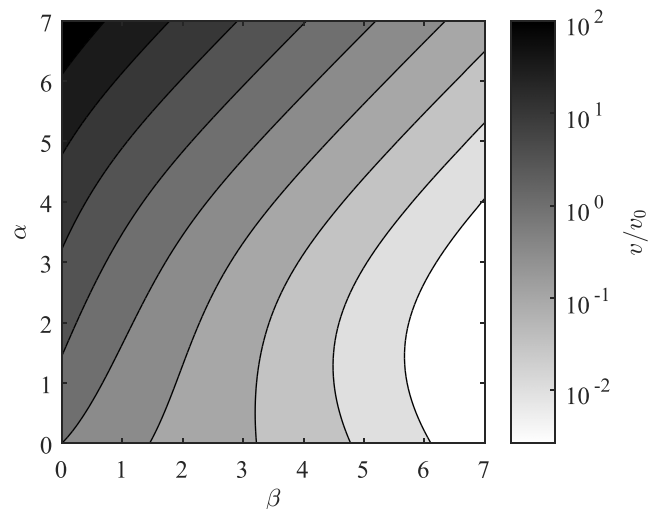

FIG. 12. Contour plots of the steady-state drift (logarithmic scale) calculated via the Gutzwiller approximation as a function of the on-site, α, and nearest-neighbor, β, interaction strength. The parameters used are $L = 1$, $\rho = 1.1$, and $\kappa_+/\kappa_- = 1.2$.

fluctuations are still suppressed, the finite number fluctuations at noninteger densities allow a limited type of hopping to occur [essentially hopping that keeps the number difference between two sites, $\hat{n}_i - \hat{n}_{i\pm1}$, constant, cf. Eqs. (7) and (8)], and a finite drift is observed. Note that a different interpretation is needed away from the $\beta \gg 1$ limit. In this case, the approximation given by Eq. (45) becomes invalid for calculating the drift (similar to the $\beta = 0$ case studied in Sec. IV B) as, in this case, number states with small coefficients can make a large contribution to the drift.

D. Comparison with the Bose-Hubbard model

It is interesting to contrast the behavior of this Brownian system with the behavior of the quantum Bose-Hubbard model. The Bose-Hubbard Hamiltonian in one dimension is given by [22]

$$\hat{H} = -J\sum_i(\hat{a}_i^\dagger\hat{a}_{i+1} + \hat{a}_{i+1}^\dagger\hat{a}_i) + \frac{1}{2}U\sum_i\hat{n}_i(\hat{n}_i - 1), \quad (49)$$

where J is the hopping matrix element for the neighboring sites i and $i + 1$ and U is the strength of an on-site interaction.

The ground state of the system is given by $\hat{H}|\psi_0\rangle = \epsilon_0|\psi_0\rangle$, where ϵ_0 is the lowest eigenvalue. The ground-state behavior of this system is interesting. In the limit of strong on-site interactions, $U/J \to \infty$, the Bose-Hubbard model demonstrates a Mott-insulator phase at integer densities. In the limit of weak interactions, $U/J \to 0$, the Bose-Hubbard model demonstrates a superfluid phase where atoms freely tunnel between sites. The Gutzwiller approximation has been used to explore the transition between the Mott-insulator and superfluid phases [22].

This has superficial similarities to the current Brownian system. For instance, in the limit of strong repulsive interaction, $\beta \gg 1$, $\alpha = 0$, the Brownian system behaves similarly to the Mott-insulator phase of the Bose-Hubbard model, in that, the nonequilibrium steady-state drift goes to zero for $\rho \geqslant 1$. In the limit of weak interactions, $\beta \ll 1$, $\alpha = 0$, the many-body master equation shows analogous behavior to the superfluid phase seen in the Bose-Hubbard model, in that the drift has a finite value in this case.

However, there are fundamental physical differences between the two many-body systems. Most importantly, the tunneling between neighboring sites occurs via a different physical process in each case. In the quantum case, at low temperature, the hopping rate J describes a quantum tunneling process between neighboring sites. In contrast, $\kappa_\pm$ describes thermally induced hopping over neighboring barriers. When interactions occur in the Brownian case, they affect the hopping rates (by effectively raising or lowing neighboring barriers), and this is captured in the number operator dependence of the hopping rates $\kappa_\pm(\hat{n}_i, \hat{n}_{i\pm1})$. In contrast, the Bose-Hubbard model displays pure on-site interactions via the interaction strength U.

These fundamental differences are evident in the many-body behavior. In particular, in the Bose-Hubbard model, interactions reduce number fluctuations, which reduce hopping and therefore superfluidity. In contrast, in the Brownian case, the relation between the drift and number fluctuations is more complicated, with large drift sometimes being associated with small number fluctuations (see Fig. 10) and small or zero drift sometimes occurring when number fluctuations are large (see Fig. 3).

V. SUMMARY

The recently derived master equation for interacting Brownian particles on a lattice provides an opportunity to explore the behavior of this system for the whole range of interaction strengths. This master equation is not analytically solvable in general, and exact numerical solutions quickly become impossible for large numbers of states and particles. Exploiting the similarity of the many-body master equation to the Bose-Hubbard model, we have adapted the Gutzwiller approximation used for the quantum Bose-Hubbard model to the Brownian case. This has enabled us to explore the full range of interaction strengths in the Brownian master equation for large systems.

The results obtained using the adapted Gutzwiller approximation reduce to the ASEP in the limit of strong repulsive nearest-neighbor interactions (and density less than 1) and agree with analytical solutions in the noninteracting and weakly interacting cases.

We used the adapted Gutzwiller approximation, to map the nonequilibrium steady-state drift and number fluctuations for both on-site and nearest-neighbor interactions across the full range of interaction strengths and densities ρ. The number fluctuations tend to finite values with increasing interaction strength except for "fingers" of strongly suppressed fluctuations close to integer values of density, independent of whether the interactions are on-site or nearest-neighbor ones. For $\rho < 1$, the drift decays to a finite value with increasing interaction strength. For $\rho \geqslant 1$ the drift tends to zero for increasing interaction strength when nearest-neighbor interactions dominate and grows exponentially when on-site interactions dominate. In the special case when the nearest-neighbor and on-site interactions have a similar magnitude, the drift tends to a finite value for strong interactions except for regions of strongly suppressed drift close to integer values of density. These last results may have application in areas where the misanthrope process has been applied, such as traffic modeling [5,16].

The approach described here can be straightforwardly extended to treat longer-range interactions, higher dimensions, and nonuniform systems. In this paper we have not considered "attachment" and "detachment" [1,32]; however, the annihilation and creation formalism lends itself to incorporating these processes.

The accuracy of the results obtained using the adapted Gutzwiller approach could be explored by comparison with results from Monte Carlo simulations, similar to the quantum case [33]. Using Monte Carlo simulations, we should be able to obtain results for systems with more particles and sites than using numerical diagonalization. This would be particularly valuable to improving the comparisons between finite-sized systems and the Gutzwiller approximation shown in Figs. 2, 8, and 9.

More broadly, this work provides an illustration of using the formal similarity between a many-body classical system and an analogous quantum system to exploit solution methods

developed over many decades for quantum systems [19]. The formulation of the interacting Brownian system in terms of creation and annihilation operators makes the adoption of these methods particularly straightforward. Due to the broader interest in nonequilibrium Brownian systems, such as in the field of active matter [34–36], for example, this could be a fruitful approach.

APPENDIX: GUTZWILLER STATE

In this Appendix we present some partial analytical results for the Gutzwiller state. Equation (23) can be written in the factorized form $\hat{\mathcal{L}}_i^{\mathrm{eff}} = \hat{L}_i \hat{R}_i$, where

$$\hat{L}_i = (\kappa_+ + \kappa_-)(\sqrt{\rho} - \hat{a}_i^\dagger), \tag{A1}$$

$$\hat{R}_i = \left(\gamma_1 e^{\alpha \hat{n}_i} \hat{a}_i - \gamma_2 e^{-\beta \hat{n}_i}\right). \tag{A2}$$

Due to this factorization the ground state of the system can be written as $\hat{R}_i |\phi_0\rangle_i = 0$ or

$$\left(\gamma_1 e^{\alpha \hat{n}_i} \hat{a}_i - \gamma_2 e^{-\beta \hat{n}_i}\right)|\phi_0\rangle_i = 0. \tag{A3}$$

Rearranging, we can write this as

$$e^{(\alpha+\beta)\hat{n}_i} \hat{a}_i |\phi_0\rangle_i = \frac{\gamma_2}{\gamma_1} |\phi_0\rangle_i. \tag{A4}$$

It is straightforward to show that the operators $\hat{A}_i = e^{s\hat{n}_i} \hat{a}_i$ and $\hat{A}_i^\dagger = \hat{a}_i^\dagger e^{-s\hat{n}}$ satisfy bosonic commutation relations: $[\hat{A}_i, \hat{A}_i^\dagger] = 1$. We can thus conclude that the $|\phi_0\rangle_i$ must be a coherent state with respect to the operator $\hat{A}_i$, and we can write

$$|\phi_0\rangle_i = \mathcal{N}^{-1} \exp\left\{\frac{\gamma_2}{\gamma_1} \hat{a}_i^\dagger e^{-(\alpha+\beta)\hat{n}}\right\} |0\rangle_i, \tag{A5}$$

where $\mathcal{N}$ is determined by the normalization condition $\langle q_0|\phi_0\rangle_i = 1$. Equation (A5) represents only a partial analytical solution as γ_1 and γ_2 need to be determined by some other means; however, it does provide information about the form of the state. In particular, since the density is given by

$$\langle q_0|_i \hat{n}_i |\phi_0\rangle_i = \rho, \tag{A6}$$

this fixes the remaining unknown parameter, the ratio γ_2/γ_1. Thus the form of Eq. (A5) tells us that for a fixed density the Gutzwiller ground state depends only on the sum $\alpha + \beta$.

Equation (14) expands the Gutzwiller state in terms of number states. It is interesting to see how the coefficients c_i^n relate to the probability of occupying the nth number state. Following from the definition of the average (5), the probability of occupying the nth number state is given by the expectation value of $|n\rangle\langle n|$, i.e.,

$$p_i^n = \langle q_0|n\rangle_i \langle n|\phi_0\rangle_i, \tag{A7}$$

where, from Eq. (14), we can recognize $c_i^n = \langle n||\phi_0\rangle_i$. From the number representation of the coherent states and Eqs. (A5) and (22) we can determine

$$\langle q_0|n\rangle_i = \sqrt{\frac{\rho^n}{n!}}, \tag{A8}$$

$$\langle n|\phi_0\rangle_i = \mathcal{N}^{-1} \frac{1}{\sqrt{n!}} \left(\frac{\gamma_2}{\gamma_1}\right)^n \exp\left\{-\frac{1}{2}(\alpha+\beta)n(n-1)\right\}. \tag{A9}$$

Combining, we find

$$p_i^n = \mathcal{N}^{-1} \frac{1}{n!} \left(\frac{\sqrt{\rho}\gamma_2}{\gamma_1}\right)^n \exp\left\{-\frac{1}{2}(\alpha+\beta)n(n-1)\right\}, \tag{A10}$$

where the normalization coefficient $\mathcal{N}^{-1}$ ensures that $\sum_n p_i^n = 1$. When $\beta = \alpha = 0$, this reduces to the Poisson number distribution characteristic of a coherent state: $p_i^n \propto \rho^n/n!$. For nonzero interaction strengths, the exponential factor leads to a reduction in number fluctuations.

Let us consider the case where $\beta \gg 1$. In this case, Eq. (A9) suggests, and Fig. 6 shows, that the number fluctuations are suppressed. In this case, assuming a density $n \leqslant \rho \leqslant n+1$, we can approximate the Gutzwiller state by just the two number states $|n\rangle$ and $|n+1\rangle$ as shown in Eq. (45). The two unknown coefficients can be determined from the normalization $\langle q_0||\phi_0\rangle_i = 1$ and the density given by Eq. (A6). This gives the result

$$|\phi_0\rangle_i = \sqrt{\frac{n!}{\rho^n}} \left\{(1+n-\rho)|n\rangle + \sqrt{\frac{1+n}{\rho}}(\rho-n)|n+1\rangle\right\}. \tag{A11}$$

We can use Eq. (A11) to evaluate γ_1 and γ_2 via Eqs. (18) and (20). We find

$$\gamma_1 = e^{-\beta n}[(1+n-\rho) + (\rho-n)e^{-\beta}], \tag{A12}$$

$$\gamma_2 = \frac{e^{\alpha n}}{\sqrt{\rho}}[n(1+n-\rho)e^{-\alpha} + (1+n)(\rho-n)]. \tag{A13}$$

Equation (A9) can be used to show that these results are consistent with the form of Eq. (A5) in the strong-interaction limit. Combining Eqs. (A12) and (A13) via Eq. (26) and dropping terms that are small when $\beta \gg 1$, we get the drift

$$v = \frac{v_0}{\rho} e^{-(\beta-\alpha)n}(1+n-\rho)[n(1+n-\rho)e^{-\alpha}$$
$$+ (1+n)(\rho-n)]. \tag{A14}$$

In both cases of interest, $\beta \gg \alpha$ or $\beta \sim \alpha$, this reduces to Eq. (47).

Using Eq. (A11), we can also calculate the quantity

$$\langle \hat{n}^2\rangle = n^2(1+n-\rho) + (1+n)^2(\rho-n) \tag{A15}$$
$$= \rho - n(1+n), \tag{A16}$$

which can be combined with $\langle \hat{n}\rangle = \rho$ to give the number fluctuations shown in Eq. (46).

[1] T. Chou, T. K. Mallick, and R. K. P. Zia, Rep. Prog. Phys. **74**, 116601 (2011).

[2] O. Campas, Y. Kafri, K. B. Zeldovich, J. Casademunt, and J. F. Joanny, Phys. Rev. Lett. **97**, 038101 (2006).

[3] A. Parmeggiani, T. Franosch, and E. Frey, Phys. Rev. Lett. **90**, 086601 (2003).

[4] K. Nelissen, V. R. Misko, and F. M. Peeters, Europhys. Lett. **80**, 56004 (2007).

[5] M. Kanai, Phys. Rev. E **82**, 066107 (2010).

[6] D. Helbing, Rev. Mod. Phys. **73**, 1067 (2001).

[7] A. Sopasakis and M. A. Katsoulakis, SIAM J. Appl. Math. **66**, 921 (2006).

[8] M. R. Evans and T. Hanney, J. Phys. A: Math. Gen. **38**, R195 (2005).

[9] M. W. Jack and A. Deaker, Phys. Rev. E **105**, 054150 (2022).

[10] C. T. MacDonald, J. H. Gibbs, and A. C. Pipkin, Biopolymers **6**, 1 (1968).

[11] A. Schadschneider, D. Chowdhury, and K. Nishinari, *Stochastic Transport in Complex Systems: From Molecules to Vehicles* (Elsevier, Amsterdam, 2011).

[12] F. Spitzer, Adv. Math. **5**, 246 (1970).

[13] J. M. J. van Leeuwen and A. Kooiman, Phys. A (Amsterdam) **184**, 79 (1992).

[14] J. M. Carlson, E. R. Grannan, and G. H. Swindle, Phys. Rev. E **47**, 93 (1993).

[15] M. R. Evans and B. Waclaw, J. Phys. A: Math. Theor. **47**, 095001 (2014).

[16] A. Tordeux, M. Roussignol, J. P. Lebacque, and S. Lassarre, Transportmetrica A: Transp. Sci. **10**, 350 (2014).

[17] M. Doi, J. Phys. A: Math. Gen. **9**, 1465 (1976).

[18] L. Peliti, J. Phys. France **46**, 1469 (1985).

[19] A. L. Fetter and J. D. Walecka, *Quantum Theory of Many-Particle Systems* (Dover, Mineola, NY, 2003).

[20] D. van Oosten, P. van der Straten, and H. T. C. Stoof, Phys. Rev. A **63**, 053601 (2001).

[21] M. C. Gutzwiller, Phys. Rev. **137**, A1726 (1965).

[22] D. Jaksch, C. Bruder, J. I. Cirac, C. W. Gardiner, and P. Zoller, Phys. Rev. Lett. **81**, 3108 (1998).

[23] M. Yamashita and M. W. Jack, Phys. Rev. A **79**, 023609 (2009).

[24] F. van Wijland and Z. Rácz, J. Stat. Phys. **118**, 27 (2005).

[25] W. Zwerger, J. Opt. B **5**, S9 (2003).

[26] M. W. Jack and M. Yamashita, Phys. Rev. A **71**, 023610 (2005).

[27] K. Sheshadri, H. R. Krishnamurthy, R. Pandit, and T. V. Ramakrishnan, Europhys. Lett. **22**, 257 (1993).

[28] E. Levine, D. Mukamel, and G. M. Schütz, J. Stat. Phys. **120**, 759 (2005).

[29] R. Rajesh and S. N. Majumdar, J. Stat. Phys. **99**, 943 (2000).

[30] N. Golubeva and A. Imparato, Phys. Rev. E **88**, 012114 (2013).

[31] T. Seppäläinen, Ann. Probab. **27**, 361 (1999).

[32] A. Parmeggiani, T. Franosch, and E. Frey, Phys. Rev. E **70**, 046101 (2004).

[33] J. Zakrzewski, Phys. Rev. A **71**, 043601 (2005).

[34] T. Speck, Europhys. Lett. **114**, 30006 (2016).

[35] M. C. Marchetti, Y. Fily, S. Henkes, A. Patch, and D. Yllanes, Curr. Opin. Colloid Interface Sci. **21**, 34 (2016).

[36] D. Needleman and Z. Dogic, Nat. Rev. Mater. **2**, 17048 (2017).